

Accepted Manuscript

A reversibly transformable chromatic system of the (octaethylporphyrin)-(dihexylbithiophene)-(Lewis base) triads. An evaluation of stereo-electronically controlled effects of dihexylbithiophene and Lewis base on its sensitivity and stability to trifluoroacetic acid

Hideto Kempe , Junro Yoshino , Naoto Hayashi , Hiroyuki Higuchi



PII: S0040-4020(14)01715-3

DOI: [10.1016/j.tet.2014.12.025](https://doi.org/10.1016/j.tet.2014.12.025)

Reference: TET 26246

To appear in: *Tetrahedron*

Received Date: 10 October 2014

Revised Date: 1 December 2014

Accepted Date: 6 December 2014

Please cite this article as: Kempe H, Yoshino J, Hayashi N, Higuchi H, A reversibly transformable chromatic system of the (octaethylporphyrin)-(dihexylbithiophene)-(Lewis base) triads. An evaluation of stereo-electronically controlled effects of dihexylbithiophene and Lewis base on its sensitivity and stability to trifluoroacetic acid, *Tetrahedron* (2015), doi: 10.1016/j.tet.2014.12.025.

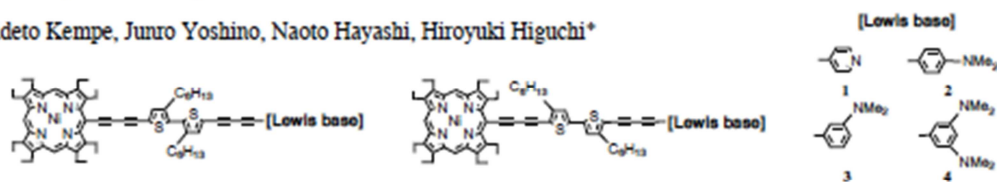
This is a PDF file of an unedited manuscript that has been accepted for publication. As a service to our customers we are providing this early version of the manuscript. The manuscript will undergo copyediting, typesetting, and review of the resulting proof before it is published in its final form. Please note that during the production process errors may be discovered which could affect the content, and all legal disclaimers that apply to the journal pertain.

PT

Graphical Abstract

A reversibly transformable chromatic system of the (octaethylporphyrin)-(dihexylbithiophene)-(Lewis base) triads. An evaluation of stereo-electronically controlled effects of dihexylbithiophene and Lewis base on its sensitivity and stability to trifluoroacetic acid

Hideto Kempe, Junro Yoshino, Naoto Hayashi, Hiroyuki Higuchi*



ACCEPTED

A reversibly transformable chromatic system of the (octaethylporphyrin)-(dihexylbithiophene)-(Lewis base) triads. An evaluation of stereo-electronically controlled effects of dihexylbithiophene and Lewis base on its sensitivity and stability to trifluoroacetic acid

Hideto Kempe,^a Junro Yoshino,^b Naoto Hayashi,^b and Hiroyuki Higuchi^{a,b,*}

^aGraduate School of Innovative Life Science, University of Toyama,

^bGraduate School of Science and Engineering, University of Toyama,

3190 Gofuku, Toyama, Toyama 930-8555, Japan

*E-mail address: higuchi@sci.u-toyama.ac.jp (H. Higuchi)

Tel/Fax: +81-(0)76-445-6616

Abstract: The extended π -electronic conjugation system of the (octaethylporphyrin)-(dihexylbithiophene)-(Lewis base) triads [OEP-DHBTh-LB] exhibits the proton-mediated reversible changes in both ¹H NMR and UV-VIS spectra via two-step processes, reflecting the structural features of DHBTh and LB constituents. The spectral changes of OEP-DHBTh-LB with trifluoroacetic acid (TFA) were quantitatively examined by means of ¹H NMR spectral measurement and comparatively analyzed in terms of stereo-electronically controlled effects of DHBTh and LB constituents on its reversibly transformable chromatic system. Successively, based on the minimum amount of TFA necessary for completion of spectral changes at respective steps, the sensitivity and stability of OEP-DHBTh-LB to TFA were evaluated, from the viewpoint of the interactive behavior of the lone pair electrons on N atom in LB with the extended OEP constituent. The present study provides a useful guideline of the molecular design for further sophisticated OEP-based chromatic system with proton-sensing functionality.

Key words: octaethylporphyrin, dihexylbithiophene, Lewis base, TFA,

lone pair electrons, chromatic system

Introduction

Over the last half a century, a great deal of effort has been continuously paid for the construction of porphyrin-based system and the like to develop the new organic functional materials, for example, a reversibly transformable molecular system between well-defined structures in an equilibrium state by means of various outside stimuli such as electronic and photonic operations.¹ In relation with functional materials science aiming at such a reversibly transformable molecular system, we have been also engaged in the studies of light-, heat-, and proton-mediated molecular behaviors.² Among them, designing our original functional porphyrin-based derivatives with proton-mediated spectral changes, we synthesized the (octaethylporphyrin)-(dihexylbithiophene)-(pyridin-4-yl) triad **1** [OEP-DHBTh-(4)Py] and preliminarily reported its functional behavior (Chart 1).³ The three constituents in **1** are simply connected with the rigid but mobile linkage of 1,3-butadiyne (diacetylene), which is useful not only for well-definition of these constituents in this system but also for extension of π -electronic conjugation with various π -electronic system (π ES). In the OEP-DHBTh-(4)Py triad, it was shown that on adding trifluoroacetic acid (TFA) into its chloroform solutions, both ¹H NMR and electronic absorption spectra regularly changed via two-step processes, reflecting the conjugation planarity related with an orientation (head-to-head; HH or tail-to-tail; TT) of two 3-hexylthiophene rings in DHBTh.^{4,5} In both spectral measurements, the first-step process corresponds to the change due to the simple protonation of TFA on N atom of Py and the second-step process to the change due to the direct affection of TFA toward OEP ring, respectively (see section 3). It was also revealed that the original spectra of **1** are recovered by quenching TFA with ordinary bases like triethylamine (Et₃N). As compared with the Py derivative **1**, the corresponding *N,N*-dimethylaminobenzene derivative **2**⁶ [OEP-DHBTh-(4)DMAB] was also examined to ascertain the generality of those phenomena, proving that both **1** and **2** are the OEP-based chromatic system with the proton-mediated transformable function via two-step processes (Chart 1).

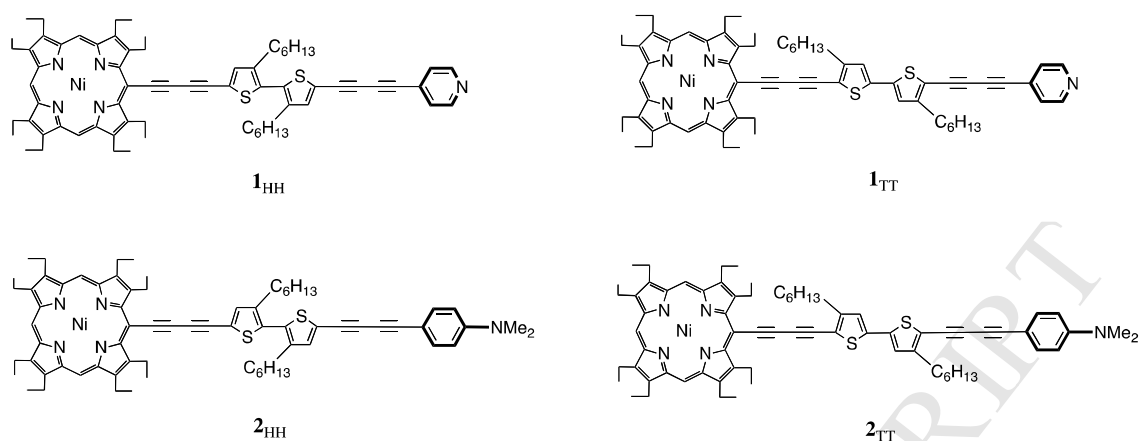
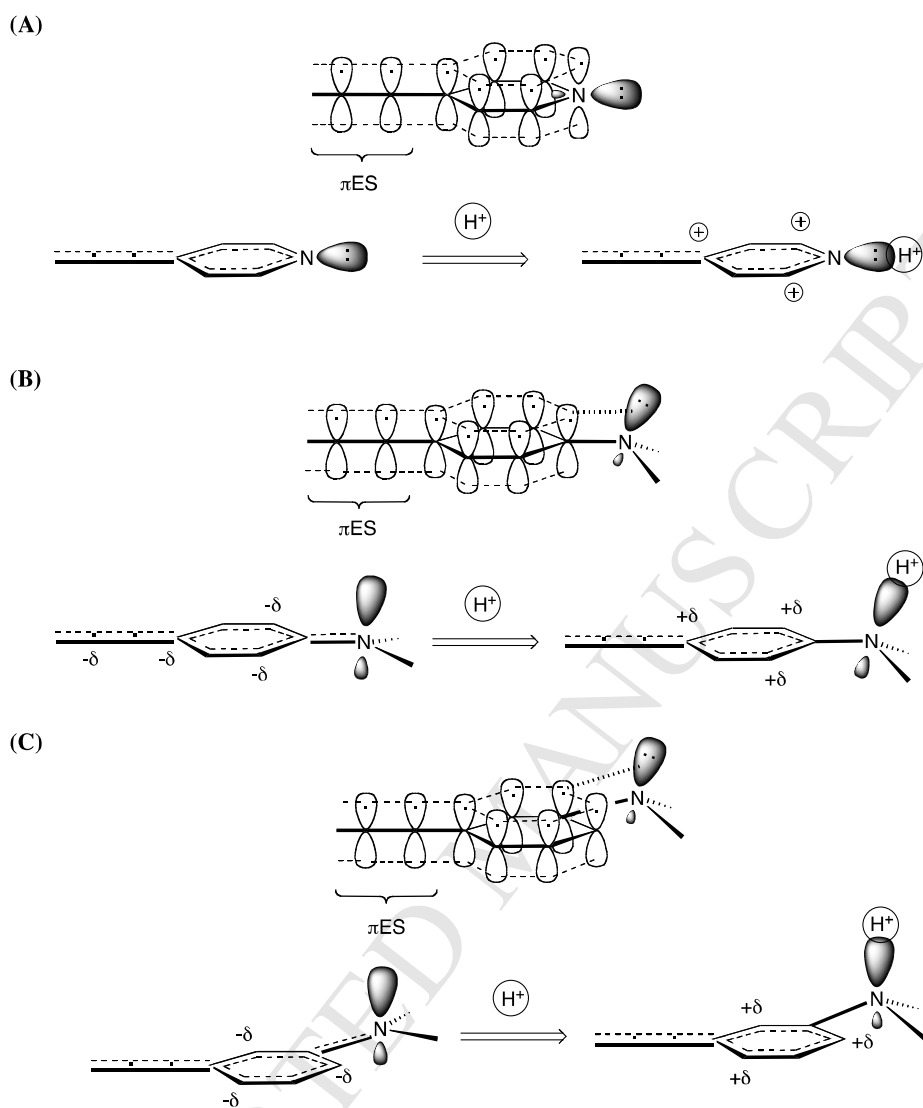


Chart 1

As expected, the sensitivity of **1** and **2** to TFA in their spectral changes at each step was apparently different between them, depending on the nature of lone pair electrons on N atom in Py and DMAB as well as an orientation of DHBTh (Chart 2). Even though the N-protonated species of Py and DMAB, *i.e.*, these conjugated acids themselves possess almost the same pK_a value as each other (5.14 for Py- H^+ and 5.06 for DMAB- H^+),⁷ ca. 10 times amount of TFA (pK_a 0.23)⁷ was necessary for completion of the first-step process in the 1H NMR spectral measurement for **2**, as compared with the necessary amount of TFA for **1**. As deduced from both residential orbital for the lone pair electrons and their conjugationally movable area (described as a delta minus in Chart 2), this result clearly indicates that the basicity (proton-accepting ability) of N atom as a Lewis base (LB) in this system substantially differs between them. The lone pair electrons of Py in **1** locate on N atom stubbornly, while those of DMAB in **2** take part in π -electronic conjugation with the external π ES to considerable extent to spread over the molecule before TFA protonates onto them.

On one hand, the higher the proton-sensing ability is attained, the lower the reversible stability is accompanied, since the cationic species formed by N-protonation are generally fragile under the highly acidic conditions. In fact, a large excessive amount of TFA is known to proceed to an extrusion reaction of Ni^{2+} ion from the OEP ring, though gradually and slightly at room temperature,⁸ lowering the quality of reversible stability as a material function in consequence (*vide supra*). Accordingly, it is very important to derive a guideline of molecular design for further enhancement of the reversible stability together with the proton-sensing ability.



(A) pyridin-4-yl, (B) anilin-4-yl, and (C) anilin-3-yl π ES. (left side) behavior of lone pair electrons before N-protonation, (right side) distribution of electron-deficient sites after N-protonation.

Chart 2

In our continuous investigations of the OEP-based chromatic system, in order to search for the structural requirements for such molecular design through the structure-property relationships, the derivatives **3** and **4** with HH- and TT-orientational DHBTh constituents have been synthesized, in which the amino group as a proton-accepting site of DMAB is attached at 3- and/or 5-positions to the external conjugation system (Chart 3). In both cases of **3** [OEP-DHBTh-(3)DMAB] and **4** [OEP-DHBTh-(3,5)DMAB], the lone pair electrons do not take part in π -electronic conjugation with the external π ES, in contrast with those in **2**, just delocalizing definitely within the benzene ring (Chart 2, C). Yet, the positive charge introduced by

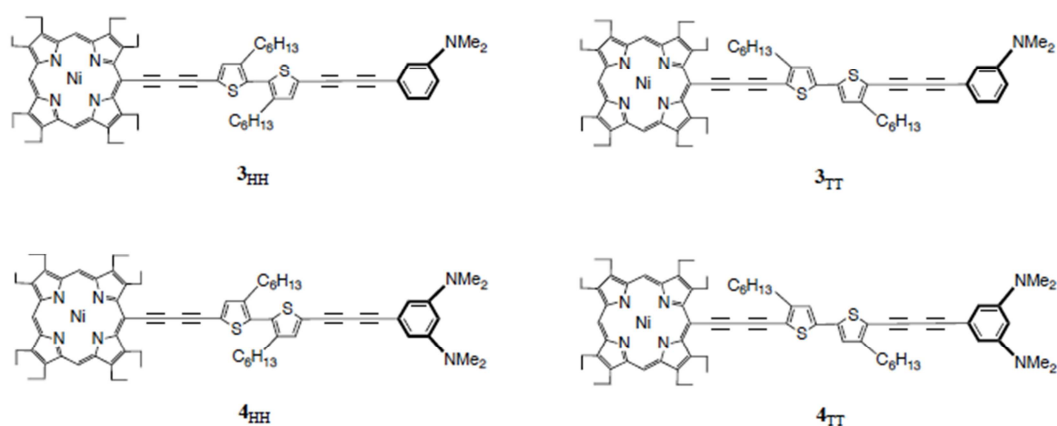


Chart 3

the protonation onto N atom of DMAB would also distribute at the definitive sites (described as a delta plus in Chart 2) on the benzene ring in **3** and **4**, conjugationally apart from the external OEP constituent, through the orbital-orbital interaction mechanism.⁹ In other words, the lone pair electrons on N atom of LB in **3** and **4** do not participate in π -electronic conjugation with the external π ES, but possess the stabilizing ability not only for themselves but also for the cationic species in a different way from the spread manner over the molecule.

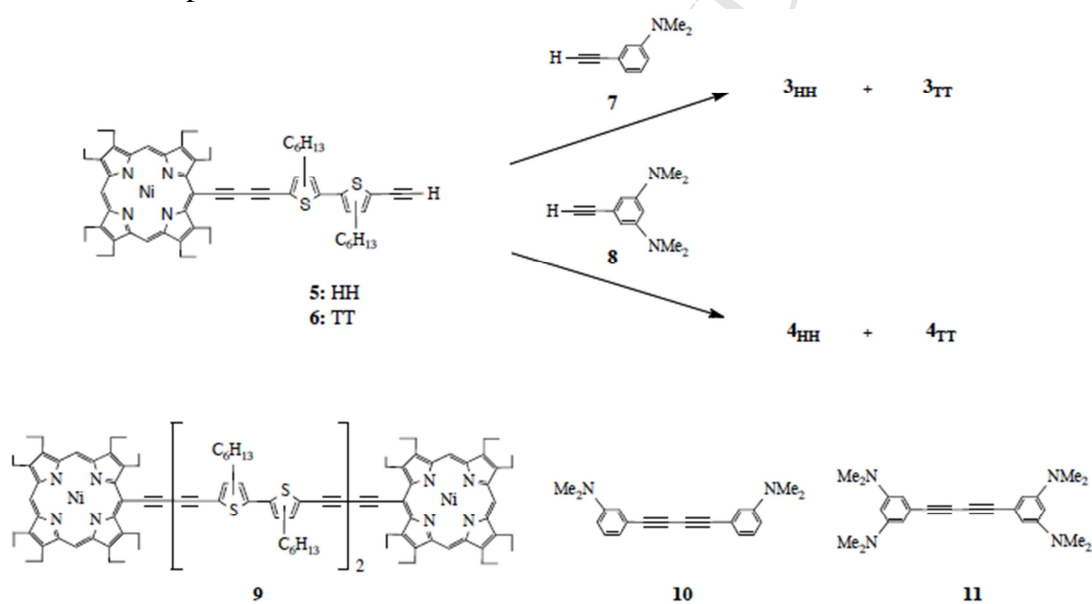
In this paper, the characteristic behaviors of **3** and **4** between before and after the N-protonation processes at each step were quantitatively examined mainly by means of ^1H NMR spectral measurements and were comparatively analyzed by the stereo-electronically controlled effects of DHBTh and LB on their spectral changes. Then, their relative sensitivity and reversible stability to TFA were evaluated, on the basis of the minimum amount of TFA necessary for completion of respective spectral changes, as compared with those of related compounds **1** and **2**. Furthermore, in the course of this study, a peculiar phenomenon was eventually observed in **4**, rightly after the completion of its first N-protonation process, distinct from **3**. From the structure-property relationships of **1-4**, a guideline of the molecular design for more sensing and stable chromatic OEP-DHBTh-LB system to TFA will be proposed.

Results and Discussions

1. Synthesis of OEP-DHBTh-DMAB **3** and **4**.

According to our conventional way,⁴ the title compounds **3** and **4** were synthesized,

by oxidative cross coupling reaction of the isomeric OEP-DHBTh acetylene **5**⁴ or **6**⁴ with corresponding DMAB acetylene **7**¹⁰ or **8**¹¹ under the modified Eglinton conditions (Scheme 1, also see Experimental part).¹² The reactions of **7** with **5** and **6** were carried out in a mixture of Py and methanol (MeOH) (5:1 in v/v) in the presence of excessive copper(II) acetate [Cu(OAc)₂]. Ordinarily, the reaction mixtures were chromatographed on silica-gel (SiO₂) column to afford the orientational isomers **3**_{HH} and **3**_{TT} in 35% and 23% yields, respectively, together with the corresponding homo-coupling dimers **9**¹³ and **10**¹⁰. The reactions of **8** with **5** and **6** under the similar conditions gave the corresponding isomers **4**_{HH} and **4**_{TT} in 28% and 32% yields, respectively, together with **9**¹³ and **11**. All the highly extended OEP derivatives **3** and **4** formed dark purple microcrystallines from CHCl₃-methanol and proved to be stable under the room light at an ambient temperature.



Scheme 1

2. ¹H NMR Spectra of OEP-DHBTh-DMAB **3** and **4**.

The spectra of **4**_{HH} as well as the corresponding reactants of terminal acetylenes **5** and **8**, for example, are shown in Fig. 1. Reflecting its skeletal feature, the spectrum of **4**_{HH} is fairly simple, similar to that of the corresponding TT-isomer. It proved that all the proton signals belonging to OEP and DMAB of **4** appeared at nearly the same chemical shifts as each other, regardless of an orientation of DHBTh, affording OEP meso-protons (meso-H) at around 9.40 ppm (3H), DMAB aromatic-protons (Ar-H) at

around 6.35 (2H) and 6.10 ppm (1H), and DMAB methyl-protons (Me-H) at around 2.95 (12H) ppm, respectively. On the other hand, the protons due to the DHBTh constituent subtly show a crucial difference in their spectral behavior between these orientational isomers. **4_{HH}** affords thiophene-protons (Th-H) at 7.28 (1H) and 7.19 (1H) ppm as a pair of singlet signals and thienylmethylene-protons (Th-CH₂) at around 2.50 (4H) ppm as a batch of signals, while **4_{TT}** affords Th-H at 6.97 (1H) and 6.94 (1H) ppm at the little higher field as a pair of singlet signals and Th-CH₂ more clearly at 2.75 (2H) and 2.65 (2H) ppm as a pair of triplet signals. These results apparently indicate that the diamagnetic ring current effect of the diacetylene linkage influences those protons closer to the triple bond to a much greater extent, such as Th-H of **4_{HH}** and Th-CH₂ of **4_{TT}**, moving them to the lower field from the corresponding protons in the opposite isomer. Such a diamagnetic ring current effect of the diacetylenic OEP constituent also slightly but firmly perturbed the particular protons of **3**, almost similar to those of **4**, except for an inherently different feature of Ar-H signals in DMAB (δ ca. 7.2 ppm (1H), ca. 6.9 ppm (2H), and ca. 6.6 ppm (1H) for both HH- and TT-isomers of **3**). Yet, it might be worthy to mention that Ar-H of **4** appeared in the higher field region by ca. 0.5 ppm than the corresponding ones of **3**, clearly indicating that the amino group efficiently increases the electron density on its *ortho*- and *para*-carbons by sending its lone pair electrons to participate into a resonant conjugation of the benzene ring, as deduced in Chart 2.

The facts obtained above evidently show that the molecular structures of **3** and **4** hold respective skeletal features of all the reactants **5**, **6**, **7**, and **8**, respectively. Thus, it concludes that since all the constituents in these derivatives **3** and **4** are connected with the rigid and straight linkage of diacetylene, the molecular skeletons are firmly defined for analytical study and are well adjusted to systematic modification of the electronic properties, which is of importance for evaluation of their functional efficiency as well. In addition, as a preliminary experimental result of **4**, it should be noted that the Ar-H signal H_b positioned between two neighboring amino groups appear at the higher field than the Ar-H signal H_a under the neutral conditions, while those H_a and H_b signals completely exchange their positions under the acidic conditions (*vide infra*).

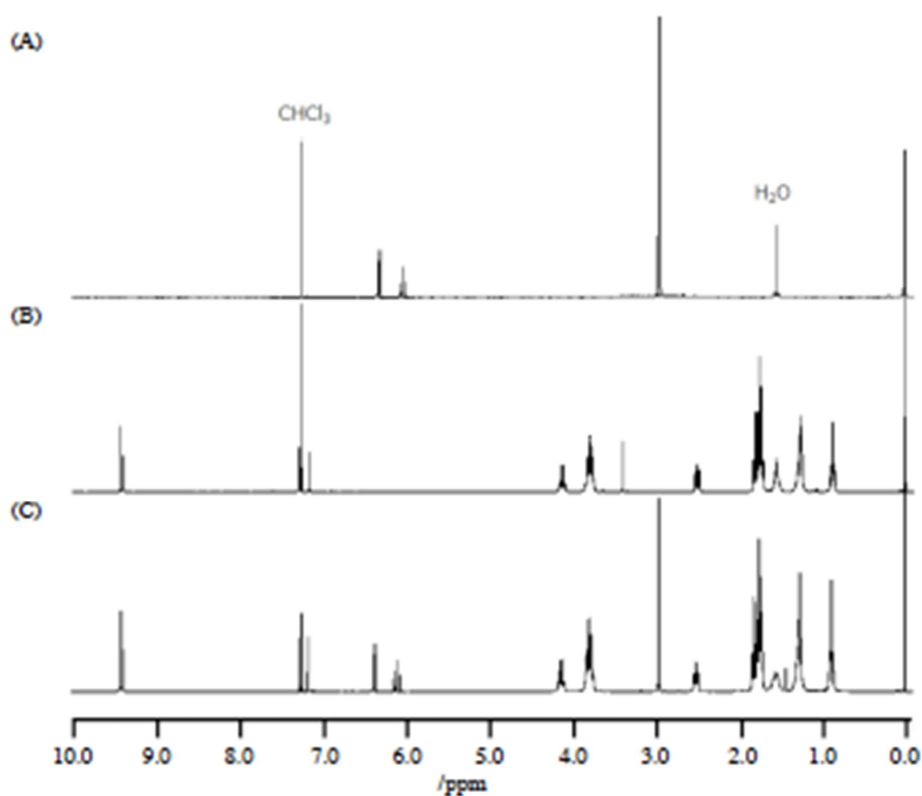


Fig. 1. ^1H NMR spectra of (A) for **8**, (B) for **5**, and (C) for **4_{HH}** (300 MHz, in CDCl_3 , 25 °C).

3. Reversible Spectral Changes of 1-4 under the Neutral and Acidic Conditions.

In the electronic absorption spectral measurements, on adding TFA into their CHCl_3 solutions (adjusted to the sample concentration of ca. $2.5 \times 10^{-5} \text{ mol}/10^3 \text{ cm}^3$ in CHCl_3 , also see Experimental part), the spectra of **3** and **4** gradually and evidently change in a visible region due to the OEP nucleus from the point at around 10^3 eq. TFA via two-step processes in common. The spectral changes are also accompanied by a striking change in color appearance of the solution from dark green to pale yellow, similar to those of **1** and **2**.^{3,6} For example, the changes of **4_{HH}** at the first-step process are just related with a gradual decrease of the intensity of Soret-Band (Fig. 2). However, the changes at the second-step process are quite complicated, mostly exhibiting a drastic reformation of Soret-Band in both intensity and absorption curve, with reflecting an orientation of DHBTh, and simultaneously giving rise to a gradual displacement of Q-Band with the new band in the much longer wavelength region. These spectral changes of **1-4** are

almost reversible, to recover the original spectra by neutralization of the TFA-containing solution with NEt_3 at any stages.

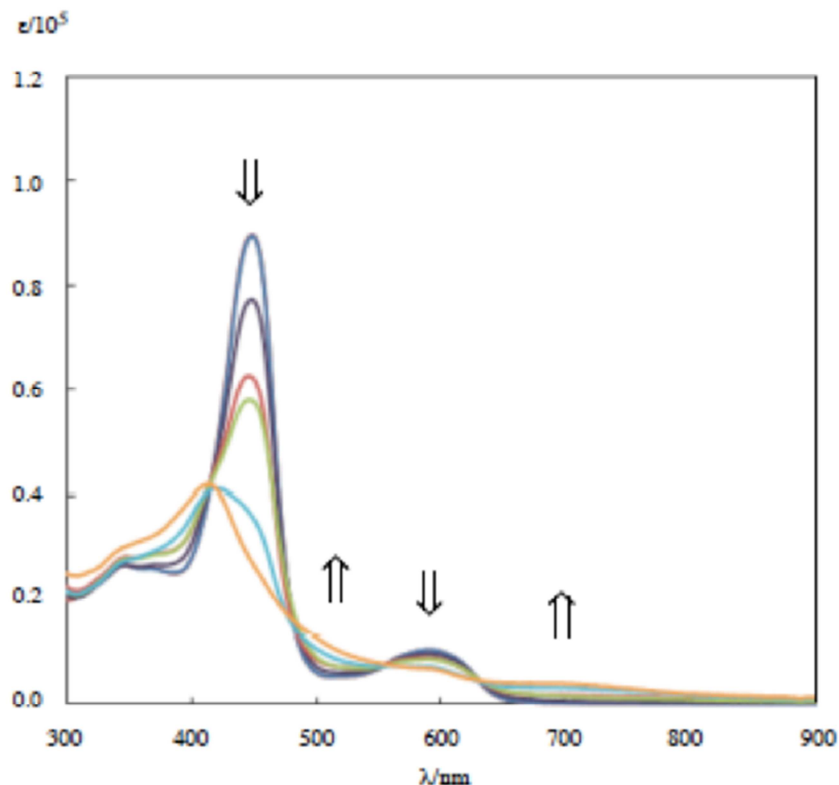


Fig. 2. Electronic absorption spectral changes with adding TFA to the CHCl_3 solution of $\mathbf{4}_{\text{HH}}$ at 25 C. The first-step: (dark blue) 1.0×10^3 eq., (purple) 1.0×10^4 eq., and (brown) 2.0×10^4 eq. to $\mathbf{4}_{\text{HH}}$. The second-step: (green) 6.0×10^4 eq., (light blue) 8.0×10^4 eq., and (orange) 1.0×10^5 eq. TFA to $\mathbf{4}_{\text{HH}}$.

Similar to such a peculiar behavior in their electronic spectral changes, ^1H NMR spectra of all the derivatives **1-4** (adjusted to the sample concentration of ca. 8.5×10^{-3} mol/ 10^3 cm 3 in CDCl_3 , also see Experimental part) also characteristically exhibit the proton/amine-mediated reversible changes via two-step processes, as seen in typical examples of $\mathbf{3}_{\text{HH}}$ (Fig. 3) and $\mathbf{4}_{\text{HH}}$ (Fig. 4). At the first-step process, all the proton signals belonging to LB just shifted to the lower field region in accordance with the added amount of TFA, with other protons belonging to both OEP and DHBTh constituents almost remained as they are. This result clearly indicates that TFA interacts first with the N atom of LB for protonation to introduce the positive charge into the LB ring, undoubtedly referring to the first-step process observed in their electronic

absorption spectra where the Soret-Band gradually weakens its intensity.

Successively after completing the N-protonation onto LB, some further excessive amount of TFA simply started to broaden the particular signals of meso-H and OEP-CH₂ without changing their chemical shifts, and then faded them out into the base line finally. An embarrassing behavior observed in these proton signals on the OEP periphery is exactly the common phenomenon at the second-step process in their ¹H NMR spectral changes, which should correspond to the drastic reformation process in the electronic structure of OEP nucleus in their electronic spectral changes. In any respects, the phenomenon at the second-step process indicates that an excess of TFA directly interacts with the OEP ring somehow.³

As shown in Fig. 3, the derivative **3_{HH}** exhibited a typical behavior of ¹H NMR spectral changes, in which on adding TFA all the Ar-H signals (δ 7.20-6.74 ppm) gradually and regularly moved to the lower field, gathered together within a narrow area of 7.7-7.5 ppm, and found their respective stationary positions after completion of the protonation onto N atom of DMAB of **3_{HH}**. Then, at the second-step process, the particular protons belonging to OEP started to broaden and finally faded out into the base line. Similarly, on adding TFA to a CDCl₃ solution of **4_{HH}** (Fig. 4), at the first-step process, the Ar-H signals due to H_a (δ 6.35 ppm) and H_b (δ 6.09 ppm) both gradually shifted to the lower field with exchanging their respective positions and then stopped moving at the stationary positions of δ 7.00 and 6.80 ppm, which was a consequence just after addition of 2 eq. TFA to **4_{HH}** (Fig. 4c). The complete reverse of H_a and H_b in chemical shift under the neutral and acidic conditions suggests that an inductive effect of the ammonium moiety on these protons is intensive enough to exceed a diamagnetic ring current effect of the triple bond, in addition to a particular feature of the H_b-linking carbon which is the synchronously neighboring position between two amino groups (Chart 2 and Chart 5, A). Anyhow, the above result of **4_{HH}** should indicate that mono(N-protonation) or bis(N-protonation) process onto DMAB was completed, as is similarly the case for the other derivatives **1-3**. However, at around 20 eq. TFA, both Ar-H signals of H_a and H_b again started moving toward the further low field region and then stopped moving at around 50 eq. TFA to reach their final stationary positions (δ 7.02 and 6.96 ppm). Moreover, at the same time, in a range between 30 eq. and 60 eq. TFA, the meso-H signals also changed to broaden and completely disappeared into the base line. A series of spectral changes observed in **4_{HH}** would lead to a rational

interpretation that the mono(N-protonation) process onto DMAB completes at 2 eq.TFA

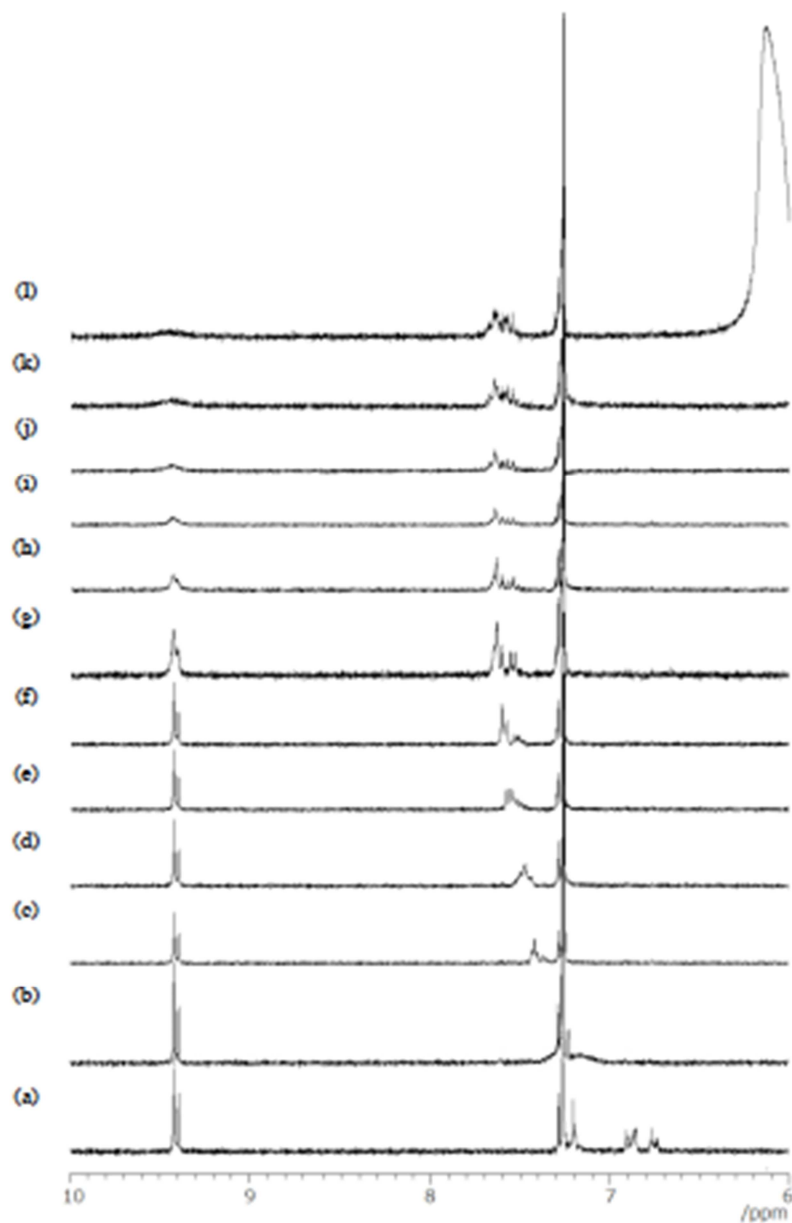


Fig. 3. ¹H NMR spectral changes in a range of 6-10 ppm with adding TFA to the CDCl₃ solution of **3_{HH}** (300 MHz at 25 C). The first-step: (a) 0 eq., (b) 1.0 eq., (c) 2.0 eq., (d) 3.0 eq., (e) 4.0 eq., and (f) 5.0 eq. TFA to **3_{HH}**. The second-step: (g) 10 eq., (h) 15 eq., (i) 20 eq., (j) 25 eq., (k) 30 eq., and (l) 35 eq. TFA to **3_{HH}**.

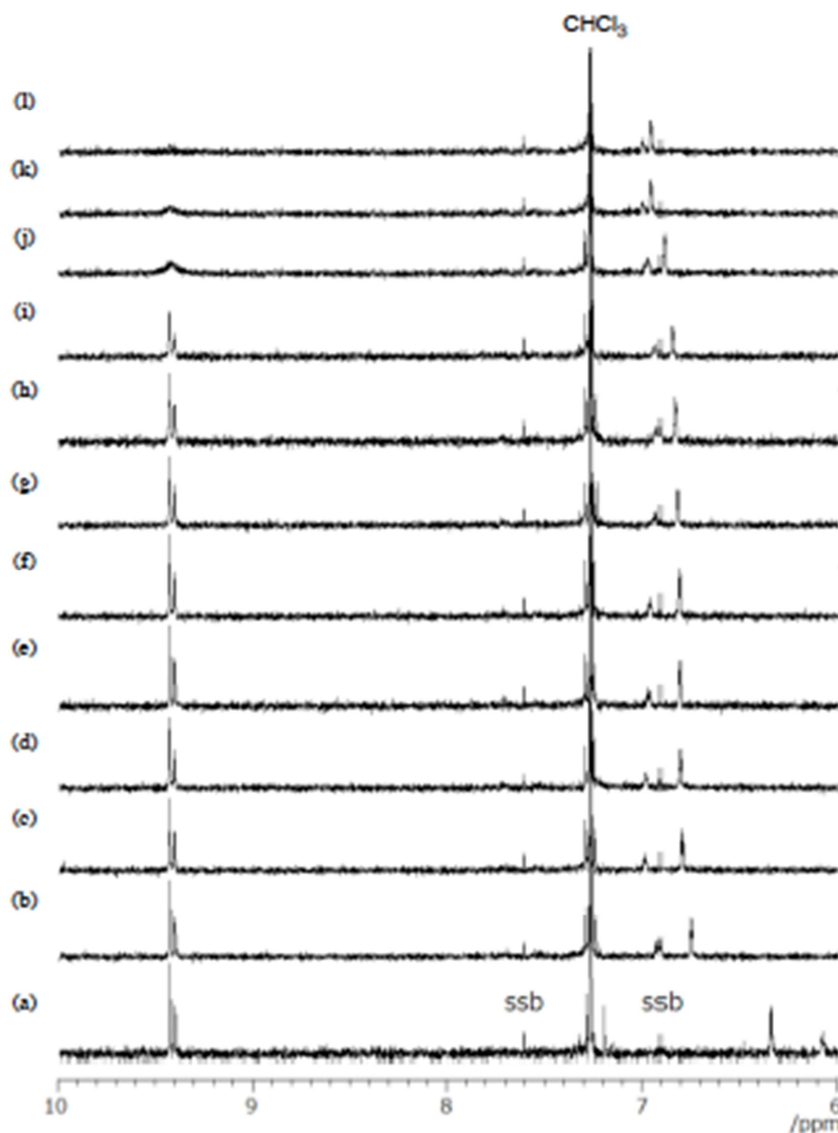
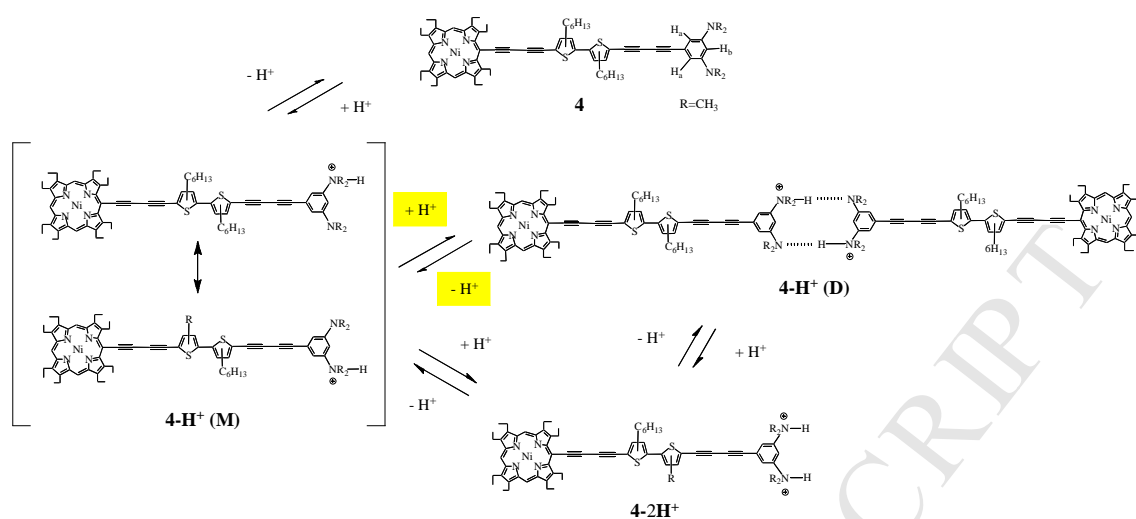


Fig. 4. ^1H NMR spectral changes in a range of 6–10 ppm with adding TFA to the CDCl_3 solution of 4_{HH} (300 MHz at 25 C). The first-step: (a) 0 eq., (b) 1.0 eq., (c) 2.0 eq., (d) 3.0 eq., (e) 4.0 eq., (f) 5.0 eq., (g) 10 eq., and (h) 20 eq. TFA to 4_{HH} . The second-step: (i) 30 eq., (j) 40 eq., (k) 50 eq., and (l) 60 eq. TFA to 4_{HH} .

and the bis(N-protonation) process starts at 20 eq. TFA and finishes at 50 eq. TFA, to reach the final equilibrium state. It is also undoubtedly indicated that the broadening and fading process of the meso-H signals of 4_{HH} starts at least after completion of the mono(N-protonation) process onto LB, similar to that of the other derivatives **1-3**. In all cases, though the OEP-DHBTh-LB system is very stable even in such a highly acidic solution, it might be wise to avoid adding TFA further unnecessarily after the point

where the meso-H signals completely disappear into the base line, in order to prevent the N-protonated species from some acid-base over-reactions (vide supra).

Although all the derivatives **1-4** exhibited the same behavior as mentioned above in common in their reversible spectral changes, regardless of orientation of DHBTh, the derivative **4** showed a peculiar behavior additionally at an intermediate stage between after completion of the mono(N-protonation) process and before start of the bis(N-protonation) process onto DMAB. Thus, on further adding TFA into the solution of the mono(N-protonated) species of **4**, the H_a signal almost retained its stationary position, while the H_b signal slightly but evidently exhibited a gradual high-field shift unexpectedly up to 20 eq. TFA (Fig. 4d-h). Fortunately, the spinning side band (ssb) signals of CHCl₃ are helpful to grasp the moving behavior of these protons in this region. Regarding this peculiar phenomenon, it is quite unlikely to presume that further addition of TFA increases the electron density on the H_b-linking carbon through π -electronic conjugation with the external π ES, because the *meta*-position to the amino substituent in **4** can not be a more electron-deficient cationic site (Chart 2). Even if it were possible somehow, the other H_a signal would also show the high-field shift similar to H_b. Alternatively, as a plausible interpretation for this curious phenomenon in **4**, an additional equilibrium between monomeric form **4-H⁺(M)** and dimeric form **4-H⁺(D)** is tentatively proposed for stabilization of the mono(N-protonated) species (Scheme 2). In such a cyclic form **4-H⁺(D)** (Chart 5B), the ring proton of H_b would be affected more intensively by a diamagnetic ring current effect of the opposite benzene ring. Thus, it would move to the higher field more or less than that in a monomeric form **4-H⁺(M)**, on adding TFA until reaching their equilibrium state. Nevertheless, since the dimeric form **4-H⁺(D)** formed by the hydrogen bonds is too fragile to hold its *metacyclophane*-like frameworks, the contribution of **4-H⁺(D)** to this equilibrium should substantially be small. In practice, the spectral changes by further adding TFA indicated that **4-H⁺(D)** readily collapses by an intramolecularly repulsive interaction between doubly-positive charges introduced by the second-step protonation onto DMAB, again generating the monomeric form **4-2H⁺** gradually and completely.



Scheme 2

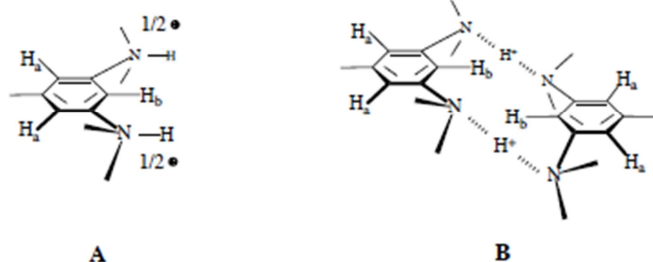


Chart 5

4. Sensitivity and Stability of 1-4 to TFA in Reversible Spectral Changes.

As mentioned briefly in section 3, the addition of TFA into CHCl_3 solution of OEP-DHBTh-LB induced to change its electronic absorption spectra in both Soret- and Q-Bands with regard to their intensity and absorption curve, and successively afforded the new bands at the longer wavelength region (Fig. 2). Among them, the selected band maxima characteristic of the OEP nucleus under the neutral and fully acidic conditions were summarized in Table 1, clearly showing that both DHBTh and LB constituents characteristically influence their maxima.

In the absence of TFA, the spectra of all the derivatives **1-4** simply exhibited almost the same behavior as each other, affording a broad Soret-Band at around 450 nm ($62.2 \text{ kcal mol}^{-1}$) for their HH derivatives and a separated Soret-Band at around 450 and 475 nm ($59.0 \text{ kcal mol}^{-1}$) for their TT derivatives.^{3,6} Similarly, the Q-Band maxima of all

Table 1. Selected absorption maxima of **OEP-DHBTh-LB** (λ_{\max}/nm , in CHCl_3)

OEP-DHBTh-LB	DHBTh	Without TFA		With TFA
		Soret-Band	Q-Band	New Band
1	HH	449	589	690
	TT	445, 476	594	725
2	HH	448	590	700
	TT	449, 478	596	730
3	HH	449	590	690
	TT	451, 474	596	712
4	HH	449	593	692
	TT	451, 476	595	709

All experiments were carried out at 25 C using the sample solutions adjusted to the concentration of ca. $2.5 \times 10^{-5} \text{ mol}/10^3 \text{ cm}^3$.

the HH derivatives appeared at around 590 nm ($47.5 \text{ kcal mol}^{-1}$), while those of the TT derivatives appeared in the longer wavelength region only by 2-6 nm ($0.15\text{-}0.50 \text{ kcal mol}^{-1}$) from the corresponding HH isomers, in consequence of the higher conjugation planarity of TT-DHBTh constituent.^{4,5} In the presence of TFA, the difference in their absorption maxima is somewhat more explicit, reflecting the structural features of both DHBTh and LB. In particular, the new bands of the three HH derivatives in **1**, **3** and **4** appeared at nearly the same maxima of 690 nm ($40.6 \text{ kcal mol}^{-1}$) as each other, while the new band of the HH derivative **2** appeared at 700 nm ($40.0 \text{ kcal mol}^{-1}$). In spite of such a suggestive behavior of the HH derivative **2**, all the TT derivatives **1-4** exhibited much longer wavelength shift and changed their new bands in an irregular trend to all appearance, affording the maxima at 725 nm ($38.6 \text{ kcal mol}^{-1}$) for **1**, 730 nm ($38.4 \text{ kcal mol}^{-1}$) for **2**, 712 nm ($39.3 \text{ kcal mol}^{-1}$) for **3**, and 709 nm ($39.5 \text{ kcal mol}^{-1}$) for **4**, respectively. As a result, the derivative **1** showed the largest energy difference ($2.0 \text{ kcal mol}^{-1}$) between HH and TT orientational isomers in their new band maxima, while the derivative **4** showed the smallest energy difference ($1.1 \text{ kcal mol}^{-1}$) between HH and TT isomers.

The spectral behavior of **1-4** under the acidic conditions should be attributed to the practical efficiency of the lone pair electrons on N atom of LB in π -electronic conjugation over the molecule, as well as to the efficient degree of π -electronic

conjugation planarity of the DHBTh constituent. In case of the derivatives **1** and **2**, the electron-deficient cationic sites of the N-protonated Py⁹ and DMAB¹⁴ rings are distributed also on the carbon directly connected with the external OEP constituent and thus potentially spread over the molecule (Chart 2, **A** and **B**), in which the conjugation planarity of DHBTh reflects severely on their stabilization efficiency. This results in a large difference of the HOMO-LUMO gap of the N-protonated species between orientational isomers. To the contrary, though the N-protonated species of **3** and **4** can be similarly stabilized by a conjugation effect in a limited area of the benzene ring, these species are in principle forbidden to bring their electron-deficient cationic sites into the external OEP constituent. Thus, the electron-deficient cationic sites are not extended across the DHBTh over the molecule, resulting in a little difference of the HOMO-LUMO gap between HH- and TT-DHBTh isomers (Chart 2). In consequence, it is proved that the derivative **1** possesses the highest sensitivity to an orientation effect of DHBTh on this system under the acidic conditions, while the derivative **4** possesses the lowest sensitivity to the DHBTh orientation. Furthermore, as compared with the differences of the new bands between **2** and **1** or **3** or **4**, regardless of orientation of DHBTh, it is evidently proved that when the lone pair electrons on N atom of LB play a cooperative role in π -electronic interaction with the extended OEP constituent both inductively and conjugationally, the new bands in this system appear in the longer wavelength region than otherwise more or less (Chart 2 and Table 1).

Table 2 shows the minimum amount of TFA necessary for completion of the respective spectral changes at each step process in the OEP-DHBTh-LB system, which was examined by ¹H NMR spectral measurements. Similar to the absorption spectral experiment, the amount of TFA in the ¹H NMR spectral experiment proved to be a very little difference between HH- and TT-DHBTh isomers, where the TT isomers needed just a bit larger amount than the corresponding HH isomers. Especially in the case of **4**, no practical difference in the amount of TFA was found between these DHBTh isomers. Such a small difference in the amount of TFA between them is probably due to the highly proton-donating ability of TFA (pK_a 0.23) to LB in the present extended OEP system (pK_a 5.14 for Py-H⁺, pK_a 5.06 for DMAB-H⁺, and $pK_{a(1)}$ 2.65 for (1,3)DMAB-2H⁺, $pK_{a(2)}$ 4.88 for (1,3)DMAB-H⁺).^{7,15} Besides, practically in order to attain the concentration of the species, at the fairly high concentrated samples of **1-4** essential for ¹H NMR spectral measurement, very small amount of TFA are enough to reach the

equilibrium state, while at the fairly low concentrated samples of **1-4** essential for absorption spectral measurement, quite large amount of TFA are necessary. Taking these facts into consideration, an adoption of the amount of TFA as a measure in accurate evaluation of the orientation effect of DHBTh on the extended OEP system is to face a technical difficulty.

Anyhow, as shown in Table 2, one is the minimum value for the first-step process corresponding to the completion of mono(N-protonation) onto LB of TT isomers of **1-4**, the other is the minimum value for the second-step process corresponding to the completion of their meso-H signal disappearance into the base line. The former can be regarded as a measure of sensitivity of this system to the acidic media, the latter as a measure of its stability in the fully acidic media, both of which are critical factors for the development of a chromatic system with the reversibly transformable functions.¹

Table 2. Minimum amount of TFA necessary for completion of the respective step processes in the TT-DHBTh derivatives of **OEP-DHBTh-LB** examined by means of ¹H NMR spectral experiments

OEP-DHBTh-LB	Role of lone pair electrons on N atom of LB	Added TFA (eq.)	
		Step 1	Step 2
1	mono-positive charge effect localization in pyridine N-atom	1.1	2.5
2	mono-positive charge effect resonance effect with the external π ES	10	25
3	mono-positive charge effect delocalization in the benzene ring	5.0	35
4	di-positive charges effect delocalization in the benzene ring	1.5	60

All experiments were carried out at 25 C using the sample solutions adjusted to the concentration of ca. 8.5×10^{-3} mol/ 10^3 cm³. The step 1 is for completion of the mono-protonation onto LB. The step 2 is for completion of the disappearance of meso-H signals.

In relation to versatile features of the lone pair electrons on N atom in LB (vide supra), several useful findings for the functional materials can be led from these results. Among **1-4**, the derivative **1** proved to be the most sensitive to TFA, in which the lone pair electrons taken in an sp² hybridized orbital do not make conjugation with any other p electrons of Py, localize rightly on N atom of LB, and thus fully play a role for

accepting a proton from TFA to bring a positive formal charge on the N atom of Py ring (Chart 2, **A**).¹⁴ As compared with **1** carrying such stubborn lone pair electrons on N atom of LB, the derivative **3** in which the lone pair electrons taken in an sp^3 hybridized orbital are unable to make conjugation with the external π ES but are able to delocalize even definitely within the benzene ring fairly lowers the sensitivity to TFA into nearly one-fifth efficiency. Similarly, as expected, the derivative **2** in which the lone pair electrons spread over the molecule through the conjugation system further lowers its sensitivity into an almost one-tenth efficiency based on **1** (Chart 2, **B** and **C**). These results apparently conclude that in order to enhance its sensitivity to TFA the lone pair electrons on N atom of LB in this system should not participate in any π -electronic conjugation as much as possible, which is exactly in a guideline for molecular design, compatible with a general principle of acid-base interaction.⁷ In this respect, it is notable that the derivative **4** showed its sensitivity to TFA almost the same as **1**. Such a high sensitivity of **4** to TFA indicates that an additional amino group to **3** can compensate sufficiently for the disadvantage in proton-accepting ability of **3** reduced by delocalization within the benzene ring, by donating the lone pair electrons from the additional N atom to the benzene ring in an opposite way (Chart 4).

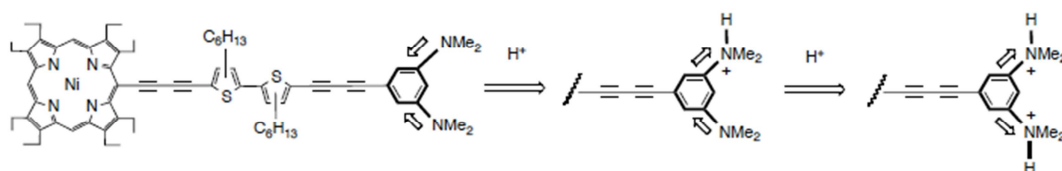


Chart 4

On the other hand, the range in reversible stability of the spectral changes proved to depend on LB much distinctly, reflecting the role of its lone pair electrons on N atom. Besides LB, taking the fact into consideration that there are several reactive π -base sites to TFA such as OEP ring, diacetylene linkage, and sulfur atom of 3HTh in the present OEP-DHBTh-LB system, the spectral reversibility of this system should be limited for an absolute guarantee up to the point where the meso-H signals completely disappear just into the base line under the fully but certain acidic conditions (see section 3).⁸ Therefore, the values at the second-step process in Table 2 represent the minimum amount necessary for each OEP-DHBTh-LB derivative reaching such a definite point under the applied conditions. Especially, the spectral changes at the second-step process

undoubtedly correspond to the direct interaction between TFA and OEP ring, after the completion of protonation onto N atom of LB, though mechanistically in a vague.^{3,6} Thus, the necessary amount of TFA would also be regarded as the strength of proton-accepting ability of OEP ring as a Lewis base in the N-protonated species of LB of this system. The smaller value corresponds to the higher proton-accepting ability of OEP ring, resulting in the less reversible stability of the system, and vice versa. In other words, the effect of cationic LB at one terminal position on the electron-donating ability of OEP ring at another terminal position in this system is to be evaluated by the amount of TFA necessary for completion of the second-step process.

Since the broadening of meso-H signals starts at least after completion of the mono-protonation on N atom in LB (section 3), it might be natural that the derivative **1** with the most sensitive to TFA shows the least stability to TFA in reverse. In case of the mono-protonated species from **2**, its stability increased into 10 times efficiency based on **1**, due to the effective delocalization of electron-deficient cationic sites up to the OEP ring through the conjugation effect (Chart 2, **B**). Similarly, the derivative **3** showed the higher stability to TFA than **2**, in spite of the 2 times higher sensitivity based on **2** (Chart 2, **C**). This result suggests that for stabilizing the N-protonated species of LB the delocalization of the electron-deficient cationic sites in a π -electronic cyclic system of the benzene ring is more efficient than in an extended π -electronic conjugation over the molecule (Chart 6). The trend of this type in stabilizing the N-protonated species was observed much further efficiently in the derivative **4**, resulting in more than 2 times higher stability based on **2** and ca. 25 times higher stability based on **1**, respectively.

Under such acidic conditions, the Lewis base strength of OEP ring in this system is to be weakened resonantly by a cationic conjugation system over the molecule, but much further efficiently by a cationic benzenoid system like an electron-withdrawing substituent to the extended OEP constituent (Chart 6). Especially in the case of **4**, it is again stressed that an additional amino substituent to **3** at the *meta*-position stabilizes the electron-deficient cationic sites specifically. And yet, since the broadening process of meso-H signal and the bis(N-protonation) step onto DMAB start almost simultaneously in the present mono(N-protonated) species, the DMAB carrying two ammonium moieties plays a much effective role for reduction of the Lewis base strength of OEP ring as a further intensified electron-withdrawing substituent (Charts 2 and 4). In addition, an inherent equilibrium between **4-H⁺(M)** and **4-H⁺(D)** should be

taken into consideration as one of the promising mechanisms for its stabilization (Scheme 2). As a whole, at present, it could be concluded that the stability in reversible spectral changes of the present OEP system is controlled critically not only by the stabilization efficiency for the N-protonated species of LB in the applied media, but also by the multiple N-protonation sites definitely playable in a benzenoid area.

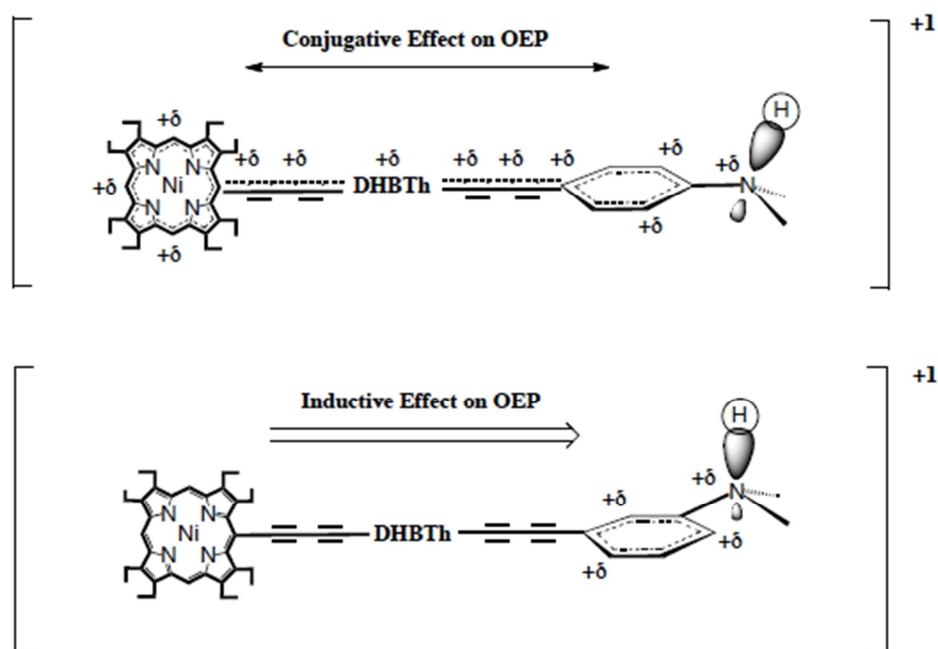


Chart 6

Conclusion

It was proved that in the OEP-DHBTh-LB system the DMAB derivative **4** possesses not only nearly the highest sensitivity but also the highest stability to TFA, with regard to the reversibly transformable spectral changes of the OEP ring. For further enhancement of its sensitivity and stability as a functional OEP derivative, the results obtained from this study provide it as a guideline for molecular design that (i) the higher proton-acceptable lone pair electrons on N atom should be incorporated into LB and (ii) the N-protonated species should stabilize its positive charge rather preferably by a delocalization in π -electronic cyclic system of the benzene ring to by an extension in π -electronic conjugation with the extended π ES constituent over the molecule. And, just recently, an electronically mobile but thermally stable 1,4-phenylene moiety like in the anthracene (Anth) ring has been found much effective for dramatic reformation of the electronic structure of the OEP ring, potentially providing a promising transmissible

spacer to respond with much smaller energy stimuli.¹⁶ Therefore, along the line obtained from this study, further study of the new OEP-Anth-LB derivatives in place of DHBTh is now in progress, aiming at further visually sophisticated proton-mediated OEP system with the much greater outputs such as chromic effect and shift.

Experimental

Melting points (Mp.) were determined on a hot-stage apparatus and are uncorrected. The EI and FAB mass spectra were recorded with a JEOL JMS-700 spectrometer, and the ESI-FT-ICR mass spectra were performed with a Bruker BioAPEX 70e spectrometer equipped with a 7 T superconducting magnet, using a sample in a solution of CHCl₃-MeOH (3:2). IR spectra were measured on a Jasco FT/IR 7300 spectrophotometer as KBr disk or neat sample; only significant absorptions are recorded in ν value (/cm⁻¹).¹⁷ ¹H NMR spectra were measured in CDCl₃ solution on a JEOL ECX-300A (300 MHz) or a JEOL JMN-EPC 600 (600 MHz) spectrometer, and were recorded in δ value (/ppm) with TMS as an internal standard, unless otherwise specified. Similarly, ¹³C NMR spectra of all the new compounds (Scheme 1) were measured on a JEOL JMN-EPC 600 (150 MHz) spectrometer, in which their signals were not certainly assigned to each carbon yet.¹⁷ The coupling constants (*J*) are given in Hz. Electronic absorption spectra were measured in CHCl₃ solution on a Shimadzu UV-2200A spectrophotometer and absorption maxima of respective bands are reported in λ_{max} value (/nm) with their extinction coefficient (ϵ) (sh=shoulder). SiO₂ (Fujisilysia BW 820MH or BW 127ZH) was used for column chromatography, unless otherwise stated. Reactions were followed with TLC on aluminum sheets precoated with Merck SiO₂ F₂₅₄ or with Merck alumina (Al₂O₃) GF₂₅₄. Organic extracts were dried over anhydrous sodium sulfate (Na₂SO₄) or magnesium sulfate (MgSO₄) prior to removal of the solvents.

All the terminal acetylenes **5-8** as the coupling reactants for the new isomeric compounds of **3** and **4** were prepared, by a tandem reaction of the corresponding bromo derivatives with trimethylsilylacetylene (TMS-acetylene) under the Sonogashira cross-coupling conditions¹⁸ and the deprotection of TMS group with K₂CO₃/MeOH, according to our conventional way.^{3,4,6} The general preparation procedure for the terminal acetylenes is shown as follows, taking a typical example of **8**.

3,5-Bis(*N,N*-dimethylamino)phenylacetylene (8): To a solution of 1-bromo-3,5-

bis(*N,N*-dimethylamino)benzene¹⁹ (544 mg, 2.3 mmol), (Ph₃P)₂PdCl₂ (32 mg, 0.045 mmol), and CuI (9.3 mg, 0.049 mmol) in diisopropylamine (20 cm³) was added TMS-acetylene (1.28 cm³, 9.5 mmol). The mixture was stirred at ambient temperature for 10 h. The reaction mixture was poured into water and extracted with CHCl₃. The extracts were washed with brine and then dried. The residue obtained after removal of the solvent was passed through a short column on SiO₂. A solution of the crude mixture was stirred in MeOH-THF (90 cm³, 2:1) containing K₂CO₃ (430 mg, 3.1 mmol) at ambient temperature under Ar atmosphere for 10 h. Poured into water, the reaction mixture extracted with CHCl₃. The residue was chromatographed on Al₂O₃ (Wako, Alumina 90) short column with ethyl acetate to afford **8** (287 mg, 68%) as brownish oil. **8**: MS (EI) *m/z* 189 (M⁺+1) for C₁₂H₁₆N₂ (MW 188.27, based on H=1.008); IR (nujol) ν 3314 (C:::CH), 2110 (C:::C); ¹H NMR δ 6.30 (2H, d, *J*=2.4, Ar-H), 6.04 (1H, t, *J*=2.4, Ar-H), 2.93 (1H, s, C:::CH), 2.92 (12H, s, NCH₃); Uv-vis λ_{max} 242 (13800), 273 (9900), 352 (4850), 395 (2250, sh) with weak absorption band tailing up to 700 nm.

5⁴: 78% yield. Dark bluish green powder (CHCl₃-methanol); Mp. 255-260 C (dec); MS (FAB) *m/z* 997.1 (M⁺+1) for C₆₂H₇₂N₄S₂Ni (MW 996.07, based on Ni=58.69); IR (KBr) ν 3310 (C:::CH), 2145 (C:::C); ¹H NMR δ 9.42 (2H, s, meso-H), 9.39 (1H, s, meso-H), 7.28 (1H, s, Th-H), 7.16 (1H, s, Th-H), 4.13 (4H, q, *J*=7, CH₂), 3.81-3.77 (12H, qm, CH₂), 3.39 (1H, s, C:::CH), 2.49 (4H, tm, Th-CH₂), 1.81-1.71, 1.25-0.87 (46H, m, CH₃ and Th-CH₂CH₂CH₂CH₂CH₂CH₃).

6⁴: 83% yield. Dark bluish green microcrystallines (CHCl₃-methanol); Mp. 273-280 C (dec); MS (FAB) *m/z* 997.0 (M⁺+1) for C₆₂H₇₂N₄S₂Ni (MW 996.07, based on Ni=58.69); IR (KBr) ν 3300 (C:::CH), 2140 (C:::C); ¹H NMR δ 9.42 (2H, s, meso-H), 9.39 (1H, s, meso-H), 6.97 (1H, s, Th-H), 6.96 (1H, s, Th-H), 4.13 (4H, q, *J*=7, CH₂), 3.82-3.77 (12H, qm, CH₂), 3.53 (1H, s, C:::CH), 2.77 (2H, t, *J*=7, Th-CH₂), 2.67 (2H, t, *J*=7, Th-CH₂), 1.81-1.72, 1.66-0.87 (46H, m, CH₃ and Th-CH₂CH₂CH₂CH₂CH₂CH₃).

7¹⁰: 77% yield. Pale yellow oil; MS (EI) *m/z* 145 (M⁺) for C₁₀H₁₁N (MW 145.20, based on H=1.008); IR (Nujol) ν 3311 (C:::CH), 2110 (C:::C); ¹H NMR; δ 7.17 (1H, td, *J*=8.1 and 0.8, Ar-H), 6.90-6.81 (2H, m, Ar-H), 6.71 (1H, br d, *J*=8.1 Ar-H), 3.01 (1H, s, C:::CH), 2.94 (6H, s, NCH₃).

All the OEP-DHBTh-DMAB isomeric derivatives of **3** and **4** were synthesized by our conventional way.⁴ As a typical reaction procedure, the synthesis of **3**_{HH} is described in the following. A mixture of **5**⁴ (80 mg, 0.08 mmol) and **7**¹⁰ (116 mg, 0.8 mmol, 10 eq. to

5) in a mixed solution of pyridine and MeOH (5:1 in v/v, 150 cm³) was added dropwise at 40 C with stirring into a solution of pyridine and MeOH (5:1, 50 cm³) containing an excessive amount of Cu(OAc)₂ (728 mg, 4.0 mmol) over 1.5 hr. Then, the reaction mixture was kept stirring at 40 C for 12 hr. Poured into water, the reaction mixture was extracted with CHCl₃. The extracts were washed with diluted HCl aq., with brine several times successively, and then dried. After removal of the solvents under reduced pressure, the residue obtained was chromatographed on SiO₂ column with hexane-CHCl₃ (4:1) as an eluent, to afford DMAB homo-dimer **10**, desired compound **3_{HH}**, and OEP-DHBTh homo-dimer **9_{HH}** in order.

10¹⁰: 33% yield (from the reaction for **3_{HH}**) and 25% yield (from the reaction for **3_{TT}**). Pale yellow plates (benzene); Mp. 160-165 C; MS (EI) m/z 288 (M⁺) for C₂₀H₂₀N₂ (MW 288.38, based on H=1.008); IR (KBr) ν 2136 (C:::C), 1593 and 1563 (C::C); ¹H NMR; δ 7.19 (2H, tm, *J*=8.5, A-H), 6.88 (2H, dm, *J*=8.5, Ar-H), 6.87 (2H, bs, Ar-H), 6.73 (2H, dm, *J*=8.5, Ar-H), 2.97 (12H, s NCH₃); Uv-vis λ_{\max} 296 (17800, sh), 313 (19800), 326 (17100) and 359 (7600, sh).

3_{HH}: 35% yield. Black purple microcrystallines (CHCl₃-methanol); Mp. over 280 C (dec); MS (FAB) m/z, 1139.0 (M⁺) for C₇₂H₈₁N₅S₂Ni (MW 1139.25, based on Ni=58.69); IR ν 2921 and 2853 (C-H), 2183 and 2130 (C:::C); ¹H NMR; δ 9.42 (2H, s, meso-H), 9.40 (1H, s, meso-H), 7.29 (1H, s, Th-H), 7.21 (1H, s, Th-H), 7.20 (1H, dd, *J*=8.0 and 7.5, Ar-H), 6.88 (1H, d, *J*=8.0, Ar-H), 6.77 (1H, br s, Ar-H), 6.74 (1H, d, *J*=7.5 Ar-H), 4.18-4.08 (4H, qm, *J*=6.5, CH₂), 3.82-3.75 (12H, qm, CH₂), 2.96 (6H, s, NCH₃), 2.52 (4H, tm, Th-CH₂), 1.82-1.70, 1.57-1.25, and 0.90-0.86 (46H, CH₃ and Th-CH₂CH₂CH₂CH₂CH₂CH₂CH₃); ¹³C NMR; δ 145.7(8), 145.0(5), 144.6(7), 143.7(5), 143.2(7), 143.0(0), 142.1(8), 140.3(3), 140.1(4), 137.7(5), 133.3(6), 130.8(8), 128.8(1), 126.6(8), 123.5(5), 120.0(8), 115.8(6), 111.3(4), 108.6(3), 107.3(5), 106.0(7), 97.9(4), 96.3(3), 93.8(8), and 92.6(3) for the sp²-C, 85.7(8), 85.6(8), 80.4(5), 78.6(4), 74.5(1), 74.1(4), 73.1(3) and 72.5(0) for the sp-C, 40.4(0), 32.1(2), 31.6(0), 31.2(7), 30.6(1), 30.3(8), 29.7(1), 28.9(6), 28.8(6), 24.5(2), 23.7(6), 22.6(9), 22.5(7), 22.4(1), 21.7(4), 19.5(4), 19.4(7), 18.1(5), 17.2(8), 14.1(3), and 14.0(7) for the sp³-C; Uv-vis λ_{\max} 346 (34800), 449 (126000), 572 (13200, sh) and 590 (14300).

9_{HH}¹³: 18% yield. Black microcrystallines (CHCl₃-methanol); Mp. over 300 C; MS (ESI-FT-ICR) m/2z 994.94 (M⁺) for C₁₂₄H₁₄₂N₈Ni₂S₄ (MW 1990.01, based on

Ni=58.69); IR (KBr) ν 2150 and 2125 (C:::C); ^1H NMR (THF- d_8) δ 9.48 (4H, s, meso-H), 9.46 (2H, s, meso-H), 7.44 (2H, s, Th-H), 7.37 (2H, s, Th-H), 4.16 (8H, q, $J=6.5$, CH_2CH_3), 3.87-3.78 (24H, qm, CH_2CH_3), 2.57-2.51 (8H, tm, Th- CH_2), 1.84-1.24 and 0.92-0.86 (92H, m, OEP- CH_2CH_3 and Th- $\text{CH}_2\text{CH}_2\text{CH}_2\text{CH}_2\text{CH}_2\text{CH}_3$).

Similarly, the oxidative cross-coupling reaction between **6**⁴ and **7**¹⁰ afforded the TT-DHBTh isomer **3**_{TT}, together with **9**_{TT} and **10**¹⁰.

3_{TT}: 23% yield. Black purple microcrystallines (CHCl_3 -methanol); Mp. over 280 C (dec); MS (FAB); m/z , 1138.9 (M^+) for $\text{C}_{72}\text{H}_{81}\text{N}_5\text{S}_2\text{Ni}$ (MW 1139.25, based on Ni=58.69); IR ν 2924 and 2868 (C-H), 2178 and 2128 (C:::C); ^1H NMR; δ 9.42 (2H, s, meso-H), 9.39 (1H, s, meso-H), 7.20 (1H, dd, $J=8.1$ and 7.5, Ar-H), 6.99 (1H, s, Th-H), 6.97 (1H, s, Th-H), 6.90 (1H, d, $J=8.1$ Ar-H), 6.87 (1H, br s, Ar-H), 6.76 (1H, d, $J=7.5$, Ar-H), 4.14-4.10 (4H, qm, CH_2), 3.82-3.75 (12H, qm, CH_2), 2.96 (6H, s, NMe-H), 2.75 (2H, t, $J=8.0$, Th- CH_2), 2.71 (2H, t, $J=8.0$, Th- CH_2), 1.82-1.71, 1.56-1.25, and 0.95-0.86 (46H, CH_3 and Th- $\text{CH}_2\text{CH}_2\text{CH}_2\text{CH}_2\text{CH}_2\text{CH}_3$); ^{13}C NMR; δ 151.9(0), 151.7(3), 150.2(2), 145.7(4), 144.9(4), 143.7(0), 142.9(8), 142.1(4), 140.3(0), 140.1(6), 137.7(8), 137.7(3), 129.1(4), 125.3(2), 125.0(8), 122.0(6), 120.5(8), 117.3(2), 116.8(8), 115.7(9), 113.7(7), 97.9(1), 97.7(8), 92.6(8) and 91.1(5) for the sp^2 -C, 86.0(1), 86.0(0), 85.0(6), 82.4(8), 81.8(1), 81.3(9), 73.8(3) and 72.9(4) for the sp -C, 40.3(6), 31.6(2), 30.2(2), 30.2(0), 30.0(0), 29.8(0), 29.7(1), 29.0(1), 28.9(0), 22.6(3), 22.6(1), 21.7(7), 19.5(3), 19.5(1), 19.5(0), 18.1(5), 18.2(0), 17.3(0), 17.2(2), 14.1(2) and 14.1(1) for the sp^3 -C; Uv-vis λ_{max} 368 (28500), 406 (46400, sh), 461 (102000), 474 (109000), 570 (14200, sh) and 596 (21800).

9_{TT}¹³: 30% yield. Black microcrystallines (CHCl_3 -methanol); Mp. over 300 C; MS (ESI-FT-ICR) m/z 994.95 (M^+) for $\text{C}_{124}\text{H}_{142}\text{N}_8\text{Ni}_2\text{S}_4$ (MW 1990.01, based on Ni=58.69); IR (KBr) ν 2150 and 2125 (C:::C); ^1H NMR (THF- d_8) δ 9.51 (4H, s, meso-H), 9.49 (2H, s, meso-H), 7.24 (2H, s, Th-H), 7.22 (2H, s, Th-H), 4.18 (8H, q, $J=6.6$, CH_2CH_3), 3.89-3.81 (24H, qm, CH_2CH_3), 2.83 (4H, t, $J=7.5$, Th- CH_2), 2.75 (4H, t, $J=7.5$, Th- CH_2), 1.85-1.29 and 0.93-0.88 (92H, m, OEP- CH_2CH_3 and Th- $\text{CH}_2\text{CH}_2\text{CH}_2\text{CH}_2\text{CH}_2\text{CH}_3$).

The derivatives of **4**_{HH} and **4**_{TT} were synthesized by the cross-coupling reaction between **8** and **5** or **6**, according to the same procedure as for the derivative **3**_{HH}.

4_{HH}: 28% yield. Black purple microcrystallines (CHCl_3 -methanol); Mp. over 280 C (dec); MS (FAB) m/z , 1181.7 (M^+) for $\text{C}_{74}\text{H}_{86}\text{N}_6\text{S}_2\text{Ni}$ (MW 1182.32, based on

Ni=58.69); IR ν 2922 and 2854 (C-H), 2182 and 2132 (C:::C); ^1H NMR δ 9.42 (2H, s, meso-H), 9.39 (1H, s, meso-H), 7.28 (1H, s, Th-H), 7.19 (1H, s, Th-H), 6.35 (1H, s, Ar-H), 6.09 (1H, s, Ar-H), 4.16-4.08 (4H, qm, CH_2), 3.82-3.77 (12H, qm, CH_2), 2.94 (12H, s, NMe-H), 2.51 (4H, tm, Th- CH_2), 1.82-1.70, 1.56-1.25, and 0.89-0.85 (46H, CH_3 and Th- $\text{CH}_2\text{CH}_2\text{CH}_2\text{CH}_2\text{CH}_2\text{CH}_3$); ^{13}C NMR; δ 145.7(8), 145.0(6), 144.4(7), 143.7(5), 142.9(9), 142.1(8), 140.3(3), 140.1(4), 137.7(5), 137.1(9), 133.3(6), 130.8(8), 128.8(1), 126.6(8), 123.5(5), 120.0(8), 115.7(9), 111.3(4), 106.0(7), 97.9(3), 97.0(2), 94.0(4), and 93.0(3) for the $\text{sp}^2\text{-C}$, 86.9(3), 86.4(8), 79.3(6), 78.7(8), 74.4(5), 74.1(4), 73.8(3) and 72.5(0) for the sp-C , 40.6(5), 31.9(3), 31.6(0), 31.2(7), 30.5(5), 30.3(8), 29.7(1), 28.9(4), 28.8(6), 24.5(2), 23.7(6), 22.6(9), 22.5(8), 22.4(1), 21.7(5), 19.5(4), 19.4(7), 18.1(4), 17.2(9), 14.1(2), and 14.0(1) for the $\text{sp}^3\text{-C}$; Uv-vis λ_{max} 352 (26500), 378 (25700), 449 (90000), 568 (14600, sh) and 593 (10500).

4_{TT}: 32% yield. Black purple microcrystallines (CHCl_3 -methanol); Mp. over 280 C (dec); MS (FAB); m/z , 1181.6 (M^+) for $\text{C}_{74}\text{H}_{86}\text{N}_6\text{S}_2\text{Ni}$ (MW 1182.32, based on Ni=58.69); IR ν 2925 and 2853 (C-H), 2178 and 2129 (C:::C); ^1H NMR δ 9.42 (2H, s, meso-H), 9.39 (1H, s, meso-H), 6.99 (1H, s, Th-H), 6.97 (1H, s, Th-H), 6.90 (1H, d, $J=8.1$ Ar-H), 6.35 (2H, br s, Ar-H), 6.08 (1H, br s, Ar-H), 4.17-4.12 (4H, qm, CH_2), 3.82-3.77 (12H, qm, CH_2), 2.95 (12H, s, NMe-H), 2.77 (2H, t, $J=8.0$, Th- CH_2), 2.72 (2H, t, $J=8.0$, Th- CH_2), 1.82-1.71, 1.57-1.25, and 0.91-0.86 (46H, CH_3 and Th- $\text{CH}_2\text{CH}_2\text{CH}_2\text{CH}_2\text{CH}_2\text{CH}_3$); ^{13}C NMR; δ 151.6(9), 151.3(4), 145.6(9), 144.8(8), 143.6(6), 142.9(2), 142.1(1), 140.2(7), 140.1(3), 137.7(3), 137.6(9), 125.2(1), 125.0(1), 122.0(9), 117.1(8), 116.9(8), 105.9(2), 98.6(7), 98.2(0), 97.8(7), 97.7(4), 92.6(6), and 91.1(5) for the $\text{sp}^2\text{-C}$, 87.1(3), 85.0(2), 82.7(8), 82.0(0), 81.4(2), 73.1(8), 71.8(9) and 67.7(7) for the sp-C , 40.6(2), 31.5(9), 30.3(5), 30.1(2), 29.9(3), 29.7(4), 29.6(9), 28.9(1), 23.7(3), 22.9(7), 22.6(1), 22.5(9), 21.7(6), 19.5(1), 19.4(8), 19.4(3), 18.1(5), 18.1(3), 17.2(2), 14.1(2) and 14.0(9) for the $\text{sp}^3\text{-C}$; Uv-vis λ_{max} 368 (19500), 406 (31400, sh), 451 (61000), 476 (66000), 570 (16100, sh) and 595 (15000).

11: 37% yield (from the reaction for **4_{HH}**) and 25% yield (from the reaction for **4_{TT}**); Pale yellow plates (CHCl_3 -hexane); Mp. 182-188 C; MS (EI) m/z , 374 (M^+) for $\text{C}_{24}\text{H}_{30}\text{N}_4$ (MW 374.52, based on H=1.008); IR ν 2139 (C:::C), 1592 and 1572 (C::C); ^1H NMR δ 6.34 (4H, d, $J=2.4$, Ar-H), 6.07 (2H, t, $J=2.4$, Ar-H), 2.93 (24H, s, NCH_3); ^{13}C NMR; δ 151.3(4), 112.4(3), 106.1(7) and 98.5(6) for the $\text{sp}^2\text{-C}$, 82.8(0) and 72.0(3)

for the sp-C, 40.6(6) for the sp³-C; Uv-vis λ_{\max} 295 (17200, sh), 322 (17500), 343 (17200) and 376 (7740, sh).

The spectral change experiments with TFA: both electronic absorption and ¹H NMR spectral measurements were carried out at 25 C, 10 min after preparation of the sample, as shown in the following procedure. For electronic absorption spectra; the 4 cm³ solutions of OEP-DHBTh-LB (**3**; 0.35 mg, **4**; 0.37 mg, both ca. 3.1 x 10⁻⁴ mmol dissolved in 10 cm³ CHCl₃) were admixed with TFA (d=1.53 g/cm³) in each equivalent ratio (Fig. 2), and then diluted with CHCl₃ to adjust their sample concentration adequate for electronic absorption spectral measurements (total 5 cm³, both ca. 2.5 x 10⁻⁵ mol/10³ cm³ for OEP- DHBTh-LB). For ¹H NMR spectra; OEP-DHBTh-LB (**3**; 4.78 mg and **4**; 5.02 mg, both ca. 4.25 x 10⁻³ mmol) was admixed with the stock solution of TFA (965 mg=8.46 mmol dissolved in 1 cm³ CDCl₃) in each equivalent ratio (Figs. 3 and 4), and then diluted with CDCl₃ to adjust their sample concentration adequate for ¹H NMR (total 0.5 cm³ CDCl₃, ca. 8.5 x 10⁻³ mol/10³ cm³ for OEP-DHBTh-LB).

Acknowledgments

Financial support by a Grant-in-Aid for Scientific Research from the Ministry of Education, Science, Sports, Culture and Technology (Nos. 23550046 and 26410039), is gratefully acknowledged. HH is also grateful to Center of Instrumental Analyses at University of Toyama for their supporting measurements of physical properties of the new compounds.

References and notes

- (a) J. A. Hill, J. M. Pratt, R. J. P. Williams, *J. Theor. Biol.*, **1962**, 3, 423-445. (b) J. H. Fuhrhop, *Tetrahedron Lett.*, **1967**, 8, 3205-3208. (c) B. Ward, C. K. Chan, Y. Richard, *J. Am. Chem. Soc.*, **1984**, 106, 3943-3950. (d) T. Shimidzu, *Supramol. Sci.*, **1996**, 3, 131-137. (e) C. M. Drain, J. T. Hupp, K. S. Suslick, M. R. Wasielewski, X. Chen, *J. Por. Phthl.*, **2002**, 6, 243-258. (f) M. A. Garcia, M. Losurdo, S. D. Wolter, W. V. Lampert, J. Bonaventura, G. Bruno, C. Yi, A. S. Brown, *Sens. Lett.*, **2008**, 6, 627-634. (g) M. Schmeisser, R. v. Eldik, *Inorg. Chem.*, **2009**, 48, 7466-7475. N. Aratani, D. Kim, A. Osuka, *Chem. Asian J.*, **2009**, 4, 1172-1182. (h) S. Sripathognak, C. J. Ziegler, M. R. Dahlby, V. N. Nemykin, *Inorg. Chem.*, **2011**, 50, 6902-6909. (i) T. Matsumoto, Y. Mitsumura, M. Miyamoto, J. Matsumoto, T. Shiragami, Y. Fueda, K. Nobuhara, M.

- Yasuda, *Anal. Sci.*, **2011**, 27, 623-628. (j) M. Mroczkiewicz, M. Pietrzak, L. Gorski, E. Malinowska, *Analyst*, **2011**, 136, 3770-3776. (k) S. Ishihara, J. P. Hill, A. Shundo, G. J. Richards, J. Labuta, K. Ohkubo, S. Fukuzumi, A. Sato, M. R. J. Elsegood, S. J. Teat, *J. Am. Chem. Soc.*, **2011**, 133, 16119-16126. (l) A. D'Urso, A. DiMauro, A. Cunsolo, R. Purrello, M. E. Fragala, *J. Phys. Chem. C*, **2013**, 117, 17659-17665. (m) D. Y. Hur, T. J. Park, E. J. Shin, *Spectrochim. Acta, Part A: Mol. Biomol. Spectr.*, **2014**, 117, 541-547. (n) M. Zhao, S. Ou, C. -D. Wu, *Acc. Chem. Res.*, **2014**, 47, 1199-1207. (o) A. K. Yetisen, M. M. Qasim, S. Nosheen, T. D. Wilkinson, C. R. Lowe, *J. Mater. Chem. C*, **2014**, 2, 3569-3576 and many other references cited therein.
2. (a) H. Higuchi, K. Takatsu, Y. Sakata, S. Misumi, T. Otsubo, *Tetrahedron Lett.*, **1982**, 23, 671-674. (b) H. Higuchi, E. Kobayashi, Y. Sakata, S. Misumi, *Tetrahaedron*, **1986**, 42, 1731-1739. (c) G. Yamamoto, H. Higuchi, H. Yamamoto, J. Ojima, *Tetrahedron Lett.*, **1991**, 32, 5129-5132. (d) G. Yamamoto, H. Higuchi, H. Yamamoto, J. Ojima, *J. Chem. Soc., Perkin Trans. 2*, **1992**, 479-487. (e) H. Higuchi, K. Shimizu, J. Ojima, K. Sugiura, Y. Sakata, *Tetrahedron Lett.*, **1995**, 36, 5359-5362. (f) H. Higuchi, S. Kiyoto, C. Sakon, N. Hiraiwa, K. Asano, S. Kondo, J. Ojima, G. Yamamoto, *Bull. Chem. Soc. Jpn.*, **1995**, 68, 3519-3538. (g) H. Higuchi, K. Shimizu, M. Takeuchi, J. Ojima, K. Sugiura, Y. Sakata, *Bull. Chem. Soc. Jpn.*, **1997**, 70, 1923-1933. (h) T. Toyama, S. Komori, J. Yoshino, N. Hayashi, H. Higuchi, *Tetrahedron Lett.*, **2013**, 54, 66-71.
3. (a) N. Hayashi, T. Matsukihira, K. Miyabayashi, M. Miyake, H. Higuchi, *Tetrahedron Lett.*, **2006**, 47, 5585-5589. (b) H. Higuchi, N. Hayashi, T. Matsukihira, T. Kawakami, T. Takizawa, J. Saito, K. Miyabayashi, M. Miyake, *Heterocycles*, **2008**, 76, 353-380.
4. N. Hayashi, A. Matsuda, E. Chikamatsu, M. Murayama, K. Mori, K. Tani, K. Miyabayashi, M. Miyake, H. Higuchi, *Tetrahedron*, **2004**, 60, 6363-6383.
5. N. Hayashi, H. Nishi, K. Morizumi, I. Kobayashi, H. Sakai, R. Akaike, K. Tani, and H. Higuchi, In *Recent Research Developments in Organic Chemistry*, ed. by S. G. Pandalai, Transworld Research Network (Kerala), 2004, Vol. 8, 401 and also see Reference 9.
6. J. Yoshino, M. Tsujiguchi, N. Hayashi, H. Higuchi, *Chem. Lett.*, **2011**, 40, 944-946.
7. (a) In "Determination of Organic Structures by Physical Methods", ed. E. D. Braude and F. C. Nachod, Academic Press (New York), 1955. (b) W. P. Jencks and J. Regenstein, in "Handbook of Biochemistry and Molecular Biology", ed. R. L.

Lundblad and F. M. MacDonald, CRC Press (New York), 4th Ed., Chapter 67; Ionization Constants of Acids and Bases, pp 595-635.

8. (a) J. W. Buchler, in "Porphyrin and Metalloporphyrins", ed. by K. M. Smith, Elsevier (Amsterdam), 1975, pp.157-231. (b) J. W. Buchler, in "The Porphyrins", ed. D. Dolphin, Academic Press (New York), 1978, pp. 389-483.

9. (a) M. J. Calhorda, R. Hoffmann, *Organomet.*, **1986**, 5, 2181-2187. (b) L. T. Scott, M. J. Cooney, C. Otte, C. Puls, T. Haumann, R. Boese, A. B. Smith III, P. J. Carroll, A. de Meijere, *J. Am. Chem. Soc.*, **1994**, 116, 10275-10283. (c) I. Novak, S. C. Ng, S. Jin, H. H. Huang, W. Huang, *J. Phys. Chem. A*, **1997**, 101, 3501-3504. (d) G. Koleva, B. Galabov, J. I. Wu, H. F. Schaefer, P. von R. Schleyer, *J. Am. Chem. Soc.*, **2009**, 131, 14722-14727.

10. J. G. Rodriguez, A. Lafuente, R. Martin-Villamil, M. P. Martinez-Alcazar, *J. Phys. Org. Chem.*, **2001**, 14, 859-868.

11. The terminal acetylene **8** was prepared by a reaction of 1-bromo-3,5-bis(*N,N*-dimethylamino)benzene¹⁹ with TMS-acetylene under the Sonogashira cross-coupling conditions.¹⁸ Also see experimental part.

12. G. Eglinton, A. R. Galbraith, *Chem. Ind.*, **1956**, 737-738.

13. H. Higuchi, T. Ishikura, K. Mori, Y. Takayama, K. Yamamoto, K. Tani, K. Miyabayashi, M. Miyake, *Bull. Chem. Soc. Jpn.*, **2001**, 74, 889-906.

14. It is well known that the electron-deficient sites (described as a circled plus in Chart 2) in the pyridinium species are distributed at the 2- and 4-positions directly, which simply spreads over the molecule through the covalent bonds in principle as an electrostatic mode (inductive effect). Only a few articles of the regioselectivity in nucleophilic reaction to the pyridinium cations are shown. (a) R. E. Lyle, D. A. Nelson, P. S. Anderson, *Tetrahedron Lett.*, **1962**, 3, 553-557. (b) R. E. Lyle, *Chem. Eng. News*, **1965**, 44, 72-78. (c) R. F. Hudson, *J. Mol. Str.; Theochem.*, **1992**, 93, 91-112. (d) G. Doddi, G. Ercolani, P. Mencarelli, *J. Org. Chem.*, **1992**, 57, 4431-4434.

15. To our best knowledge, the $pK_{a(1)}$ and $pK_{a(2)}$ values of conjugated acid 1,3-bis(*N,N*-dimethylamino)benzene are unknown yet. The pK_a value (4.58) of conjugated acid, aniline- H^+ with aniline in water at 25 C, is known to be slightly smaller, *i.e.*, a little higher acidity, as compared with that of 5.15 between DMAB and DMAB- H^+ .⁷ Thus, based on this fact, the $pK_{a(1)}$ and $pK_{a(2)}$ values of the conjugated acid of 1,3-bis(*N,N*-dimethylamino)benzene could be expected to be

slightly larger than those ($pK_{a(1)}$ 2.65 and $pK_{a(2)}$ 4.88) of corresponding conjugated acid of 1,3-phenylenediamine.⁷

16. H. Kempe, N. Kuroda, J. Yoshino, N. Hayashi, H. Higuchi, *Tetrahedron Lett.*, **2014**, 55, 5164-5169.

17. IR spectra reflect the bond-multiplicity of the molecule and ^{13}C NMR spectra reflect the electron-density on respective carbons of the molecule. In relation with the present study on the sensitivity and stability of OEP-DHBTh-LB to TFA, the results from IR and ^{13}C NMR spectra of the OEP-DHBTh-LB and OEP-Anth-LB derivatives will conclusively be discussed in the following article.

18. K. Sonogashira, Y. Tohda, N. Hagihara, *Tetrahedron Lett.*, **1975**, 4467-4470.

19. H. K. Kim, S. K. Kim, J. H. Park, S. W. Yoon, M. H. Lee, Y. Do, *Chem. Asian J.*, **2008**, 3, 1912-1921.

Figure Captions

Fig. 1. ^1H NMR spectra of (A) for **8**, (B) for **5**, and (C) for **4_{HH}** (300 MHz, in CDCl_3 , 25 C).

Fig. 2. Electronic absorption spectral changes with adding TFA to the CHCl_3 solution of **4_{HH}** at 25 C. The first-step: (dark blue) 1.0×10^3 eq., (purple) 1.0×10^4 eq., and (brown) 2.0×10^4 eq. to **4_{HH}**. The second-step: (green) 6.0×10^4 eq., (light blue) 8.0×10^4 eq., and (orange) 1.0×10^5 eq. TFA to **4_{HH}**.

Fig. 3. ^1H NMR spectral changes in a range of 6-10 ppm with adding TFA to the CDCl_3 solution of **3_{HH}** (300 MHz at 25 C). The first-step: (a) 0 eq., (b) 1.0 eq., (c) 2.0 eq., (d) 3.0 eq., (e) 4.0 eq., and (f) 5.0 eq. TFA to **3_{HH}**. The second-step: (g) 10 eq., (h) 15 eq., (i) 20 eq., (j) 25 eq., (k) 30 eq., and (l) 35 eq. TFA to **3_{HH}**.

Fig. 4. ^1H NMR spectral changes in a range of 6-10 ppm with adding TFA to the CDCl_3 solution of **4_{HH}** (300 MHz at 25 C). The first-step: (a) 0 eq., (b) 1.0 eq., (c) 2.0 eq., (d) 3.0 eq., (e) 4.0 eq., (f) 5.0 eq., (g) 10 eq., and (h) 20 eq. TFA to **4_{HH}**. The second-step: (i) 30 eq., (j) 40 eq., (k) 50 eq., and (l) 60 eq. TFA to **4_{HH}**.